LIGO SURF Progress Report 2: Studying the effects of higher-order modes on the parameter estimation of precessing low-mass binary black holes

Rupini V. Kamat,[1] Patricia Schmidt,[2] Rory Smith,[2] and Yanbei Chen[2]

[1]*LIGO SURF Student, California Institute of Technology*
[2]*LIGO SURF Mentors, California Institute of Technology*

(Dated: July 29, 2016)

I. OVERVIEW

Given LIGO's recent breakthroughs in gravitational wave detection, it has become increasingly important to optimize the parameter estimation methods used to analyze the systems observed by LIGO to ensure that the data collected by LIGO can be used to conduct meaningful astrophysical research. Standard LIGO parameter estimation uses a Bayesian approach to recover a system's physical parameters by comparing the detected signal to template waveforms at many different points in the parameter space. Current template waveforms include only a few dominant, lower-order spherical harmonic modes. However, for certain compact binary systems, particularly precessing systems and systems with high asymmetries, higher order modes carry a significant amount of energy, and thus information. In those cases, including only lower order modes in template waveforms may lead to inaccuracies in the parameter estimates. Our project seeks to determine if including higher-order modes in inspiral template waveforms for precessing, low-mass binary black hole systems has the potential to allow us to more accurately recover certain properties of an observed system through its detected gravitational waveform.

II. METHODS

First, we choose a set of precessing low-mass black hole binary systems to analyze. In addition to a total mass constraint of $\leq 12M_{\odot}$, we construct our cases by choosing systems we would expect to emit a significant amount of radiation in higher modes. From a series of match calculations done in the first weeks of the project (see first progress report for details), the systems that produce a significant amount of radiation in higher order modes have parameters in the neighborhood of mass ratio $q = 6$, dimensionless spin vectors $\vec{\chi}_1 = \vec{\chi}_2 = (0.6,\ 0,\ 0)$, and an inclination angle[11] of $\theta \approx \pi/2$. We then generate the gravitational waveforms produced by our chosen systems, both with and without higher modes. For our higher modes analysis, we will be using the post-Newtonian inspiral waveforms for precessing binary black holes given in Appendix A in Ref. [1].

We then analyze the resulting simulated waveforms in two stages: first using a Fisher information matrix analysis and then using full Bayesian parameter analysis for select cases. We use Fisher analysis to get a best estimate of the improvement in parameter uncertainty, if any, that results from the inclusion of higher waveforms. We then isolate the binary cases for which the inclusion of higher modes results in the most improvement in parameter estimation, according to our Fisher analysis, and perform full Bayesian parameter estimation, using the nested sampling algorithms in the LALInference software library, to more thoroughly quantify the effects that including higher modes has on parameter estimation.

A. Fisher Matrix Analysis

Due to the high computational cost of a Bayesian parameter estimation analysis with LALInference, we decided to begin our analysis of the effects of higher modes on parameter estimation with a Fisher matrix analysis. The Fisher information matrix is a tool that allows one to measure the amount of information that a given set of data provides about some unknown parameter that can be used to model the data set. It is defined as follows:

$$\Gamma = -[\nabla\nabla \ln(L)], \tag{1}$$

where L is the likelihood function described in Sec. II B. The inverse of the Fisher matrix gives the covariance matrix of the posterior probability distribution, where the *statistical uncertainty* of a measured parameter λ_i due to noise is given by

$$(\Delta\lambda_i)_{\rm stat} = \sqrt{\Gamma^{-1}_{ii}}, \tag{2}$$

and the remaining entries in the matrix $\Gamma_{ij} = \Gamma_{ji}$ give the correlation between two parameters λ_i and λ_j.

In the case of a gravitational wave signal, we can assume that an observed signal $s \in \mathbb{R}$ contains some noise n and a gravitational wave signal $h_0(\vec{\lambda}_{\rm true})$, where $\vec{\lambda}_{\rm true}$ are the true parameters of the observed system

$$s = n + h_0(\vec{\lambda}_{\rm true}). \tag{3}$$

Thus, if we model the signal as $h(\vec{\lambda})$, we can represent the likelihood function as the following:

$$L(s|\vec{\lambda}) \propto e^{-\langle s-h(\vec{\lambda}), s-h(\vec{\lambda})\rangle/2}, \tag{4}$$

where $\langle \bar{h}, \bar{g}\rangle$ is the overlap, or the noise-weighted inner product, of two real functions $\bar{h}(t)$ and $\bar{g}(t)$, as defined below:

$$\langle \bar{h}, \bar{g}\rangle = {\rm Re}\int_{-\infty}^{\infty} \frac{\tilde{h}(f)\tilde{g^*}(f)}{S_n(|f|)} df e^{2i(\psi-\sigma)} + {\rm Re}\int_{-\infty}^{\infty} \frac{\tilde{h^*}(-f)\tilde{g^*}(f)}{S_n(|f|)} df e^{-2i(\psi+\sigma)}, \tag{5}$$

where $h, g \in \mathbb{C}$ are the *complex* strains, $\bar{h} = {\rm Re}[h e^{2i\psi}]$ and $\bar{g} = {\rm Re}[g e^{2i\sigma}]$, where the polarization angles are ψ and σ respectively. The Fourier transform of h is denoted by $\tilde{h}$ and the complex conjugate by h^*. We use the one-sided noise power spectral density (PSD) $S_n(|f|)$ for the advanced, zero-detuned LIGO detector. The algorithm used to calculate the match is discussed in Appendix A.

From Eq.(5) we define the norm of a waveform as

$$||h|| = \sqrt{\langle h, h\rangle}, \tag{6}$$

and the normalized waveform $\hat{h}$ as

$$\hat{h}(\vec{\lambda}) = \frac{h(\vec{\lambda})}{||h||}. \tag{7}$$

If we assume that the noise in a gravitational wave signal is Gaussian with a mean of zero and that our prior probability distribution for the data is a flat distribution, the elements of the Fisher information matrix are given by:

$$\Gamma^{ij}(\vec{\lambda}) = \left\langle \frac{\partial h}{\partial \lambda_i}(\vec{\lambda}), \frac{\partial h}{\partial \lambda_j}(\vec{\lambda}) \right\rangle. \tag{8}$$

The Fisher matrix scales quadratically with SNR, which is a detection statistic that quantifies signal strength and is defined as follows:

$$\rho = \max_{\lambda} \langle s, \hat{h}(\lambda) \rangle, \tag{9}$$

where s is the observed signal and $\hat{h}$ is the normalized template waveform used to model the data.

The optimal SNR for a given gravitational waveform h is given by

$$\rho_{opt} = \langle h, h \rangle. \tag{10}$$

Thus, we can define an SNR-independent, normalized Fisher matrix as shown in Eq. 23 in Ref. [2]:

$$\hat{\Gamma}^{ij}(\vec{\lambda}) = \frac{1}{\rho^2_{opt}} \Gamma^{ij}(\lambda). \tag{11}$$

We developed code to calculate the Fisher matrix for a given gravitational waveform in `Mathematica`. Our implementation used finite differencing methods to calculate the derivative of the waveform with respect to a given parameter, as shown in Eq.(12).

$$\frac{\partial h}{\partial \lambda_i}(\vec{\lambda}) \approx \frac{h(\lambda_1, \lambda_2, ..., \lambda_i + \delta\lambda_i, ...\lambda_n) - h(\lambda_1, \lambda_2, ..., \lambda_i - \delta\lambda_i, ..., \lambda_n)}{2\,\delta\lambda_i} \tag{12}$$

It then calculated the overlap, as defined in Eq.(5), between derivatives of the waveform using the algorithm outlined in Appendix A to produce the Fisher information matrix of the waveform h. We then normalized the Fisher matrix, using Eq. 7, and assumed an SNR of $\rho = 15$ (i.e. multiplied the normalized Fisher matrix by ρ^2), as done by Cho et al. in Ref. [2]. Inverting this Fisher information matrix gives us the covariance matrix of the system, which has the following form:

$$C_{ij} = \begin{cases} \sigma_{ij} & i \neq j \\ \sigma_i^2 & i = j \end{cases}, \tag{13}$$

where σ_{ij} is the covariance between two parameters λ_i and λ_j, and σ_i is the statistical error of the parameter λ_i, as stated in Eq. (2). We can use the information in the covariance matrix of a given system's waveform to construct two dimensional confidence ellipses that show visually both how well each individual parameter is constrained, as well as how various parameters are correlated with one another. We do so by first constructing a set of 2x2 matrices of the form:

$$c(\lambda_i, \lambda_j) = \begin{pmatrix} \sigma_i^2 & \sigma_{ij} \\ \sigma_{ji} & \sigma_j^2 \end{pmatrix}, \tag{14}$$

Then, we can construct the 1σ and 2σ confidence ellipses, which correspond to confidence levels of 68.3% and 95.4% respectively. The ellipse for each confidence level represents the region in which we can

state that for repeated measurements, the probability that the true values for λ_i and λ_j lie within the ellipse is given by the confidence level. The parameters of a confidence ellipse is given by:

$$a^2 = \alpha^2 \left(\frac{\sigma_m^2 + \sigma_b^2}{2} + \sqrt{\frac{(\sigma_m^2 - \sigma_b^2)^2}{4} + \sigma_{mb}^2} \right), \tag{15}$$

$$b^2 = \alpha^2 \left(\frac{\sigma_m^2 + \sigma_b^2}{2} - \sqrt{\frac{(\sigma_m^2 - \sigma_b^2)^2}{4} + \sigma_{mb}^2} \right), \tag{16}$$

and

$$\tan(2\theta) = \frac{2\sigma_{mb}}{\sigma_m^2 - \sigma_b^2}, \tag{17}$$

where a and b are the axes of the ellipse, θ is the counterclockwise rotation of the ellipse, and α changes based on the confidence interval the ellipse to represents. For a 1σ, or 68.3%, confidence level, $\alpha = 1.52$. For a 2σ, or 95.4%, confidence level, $\alpha = 2.48$ [3].

If h is an accurate model for the system's true waveform h_0, the posterior probability distribution, or the probability distribution of parameters that would result from a thorough parameter estimation analysis, can then be approximately described by the *maximum likelihood estimate* $\vec{\lambda}'$, i.e. the set of parameters that maximize $L(s|\vec{\lambda})$, and the parameter uncertainties given by Eq.(2). If, however, the model waveform h is different from the true waveform h_0, such that

$$\delta h(t;\vec{\lambda}) = h_0(t;\vec{\lambda}) - h(t;\vec{\lambda}) \neq 0, \tag{18}$$

then the maximum likelihood estimate $\vec{\lambda}'$ for the true parameters has some *systematic* error that is not described by Eq. (2), which quantifies only the *statistical* error due to the noise. Using the derivation shown in Section 2.3.3 of Ref. [4], we find that the systematic error that arises from an incomplete waveform model is given by:

$$(\Delta\lambda_i)_{\rm sys} = [\Gamma^{-1}(\vec{\lambda}')]_{ij} \left\langle \delta h_0(\vec{\lambda}'), \frac{\partial h}{\partial \lambda_j}(\vec{\lambda}') \right\rangle. \tag{19}$$

The total error in the estimate for a single parameter is given by the sum of the statistical error and the systematic error. Because, as previously mentioned, Γ_{ij} scales quadratically with SNR, we have that $(\Delta\lambda_i)_{\rm stat}$ increases linearly with decreasing SNR, while $(\Delta\lambda_i)_{\rm sys}$ is independent of the SNR. Thus, systematic error is the dominant source of parameter estimation error at high signal-to-noise ratio (SNR), but becomes negligible compared to statistical error at low SNR.

Thus, we can define some SNR-dependent "indistinguishability criterion" to determine whether or not two different waveforms h and h_0 can be considered *indistinguishable* from one another. Following Ref. [5], we call two waveforms indistinguishable if $(\Delta\lambda)_{\rm sys} < (\Delta\lambda)_{\rm stat}$. Thus, we can use Fisher matrices to analyze whether or not the quadrupole and $\ell = 2$ waveforms of a system are "indistinguishable" from the higher-mode-inclusive waveform of the same system. This enables us to determine if there exist areas in the parameter space for low mass, precessing binary black holes where significant systematic error arises from using only quadrupole or $\ell = 2$ waveforms during parameter estimation. Once we have isolated these areas in the parameter space, we can chose a selection of binary black hole cases on which to perform a full parameter estimation analysis.

B. Bayesian Analysis

Having chosen some binary cases using a Fisher information matrix analysis, full parameter recovery on a few selected cases will be performed twice: once using the quadrupole waveforms as template waveforms and once again using higher-mode-inclusive waveforms. This will enable us to compare the results from each parameter estimation run and study the effects of including higher modes. To measure the source parameters, we will be performing a *Bayesian analysis* using the tools offered in the LALInference software library for Bayesian parameter estimation [6].

In general terms, the process of Bayesian analysis is as follows. First, a probability distribution, known as the *prior distribution* and represented as $p(\vec{\lambda})$, is constructed for each set of parameters $\vec{\lambda}$ in the binary parameter space. Each set of parameters in the binary parameter space includes values like component masses, spins, position on the sky, distance to the source, orientation of the binary, and many more. The prior distributions we will use in our project consist of uniform distributions over a given range for parameters like component masses and spin magnitudes, and isotropic distributions over the unit sphere for the spin orientation.

After a prior distribution has been constructed, the likelihood $L(s\,|\,\vec{\lambda})$ of the observed signal s given the parameters $\vec{\lambda}$ is calculated using Eq. 4. Then, we multiply the likelihood function by the prior distribution $p(\vec{\lambda})$ and normalize by $p(s)$, the probability of the signal independent of the distribution of the parameters, also known as the evidence. This gives us the posterior probability distribution, $p(\vec{\lambda}\,|\,s)$, as described by Bayes' Theorem:

$$p(\vec{\lambda}\,|\,s) = \frac{L(s\,|\,\vec{\lambda})\,p(\vec{\lambda})}{p(s)}. \tag{20}$$

The parameter estimate is then given by the median value of the posterior distribution, and the error is given by the values that correspond to the 90% credible interval, or the parameter values that enclose 90% of the probability of the distribution. We will then compare the results of the two parameter estimation runs for each binary case, and analyze how the inclusion of higher modes affects our ability to accurately constrain the parameters of the model system. This will enable us to determine whether or not the inclusion of higher modes improves the accuracy of parameter estimation in the inspiral case for precessing, low-mass black holes.

III. CURRENT STATUS OF RESULTS

In addition to the results gathered in the beginning weeks of the project, which include a set of animations that depict the time evolution of different modes of the gravitational radiation field, various match calculations between the higher-mode-inclusive and higher-mode-exclusive waveforms of different systems, and an example of Fisher matrix analysis as applied to the fitting of a straight line to noisy data, we have since begun to apply a Fisher matrix analysis to gravitational waveforms. The technical details of our implementation of this analysis are described in Section II A.

A. Aligned-spin case

We first applied the Fisher analysis to an "aligned spin case", i.e., a binary configuration for which the spins of each black hole are aligned with the orbital angular momentum of the black hole binary. In this case, no precession of the orbital plane is present, so the inspiral waveform of the system depends only on the following parameters: the mass ratio q, the initial separation a_{init}, the spin magnitude of the less massive black hole $||\vec{\chi}_1||$, and the spin magnitude of the more massive black hole $||\vec{\chi}_2||$. The total mass of the system

M_{total} and the distance to the system D_L are scaling factors that are added in later to rescale the waveform and insert physical units. This is true for the precessing case as well.

Using the method described in Section II A, we then generated Fisher information matrices and covariance matrices for the ($\ell = 2$), ($\ell = 2,3$), and ($\ell = 2,3,4$)-waveforms of a specific aligned spin system, where we only varied the mass ratio q, the dimensionless spin magnitudes $||\vec{\chi}_1||$ and $||\vec{\chi}_2||$, and inclination angle θ to calculating the Fisher information matrix. This resulted in a 4x4 covariance matrix of the following form:

$$C \equiv [\Gamma^{-1}] = \begin{pmatrix} \sigma_q^2 & \sigma_{q\chi_1} & \sigma_{q\chi_2} & \sigma_{q\theta} \\ \sigma_{\chi_1 q} & \sigma_{\chi_1}^2 & \sigma_{\chi_1\chi_2} & \sigma_{\chi_1\theta} \\ \sigma_{\chi_2 q} & \sigma_{\chi_2\chi_1} & \sigma_{\chi_2}^2 & \sigma_{\chi_2\theta} \\ \sigma_{\theta q} & \sigma_{\theta\chi_1} & \sigma_{\theta\chi_2} & \sigma_\theta^2 \end{pmatrix} \tag{21}$$

For certain parameters, we found the Fisher matrix to be ill-conditioned, i.e., resulting in negative values in the diagonals of the covariance matrix, which results in imaginary parameter uncertainties, and covariance matrices that are effectively zero. While this is expected for systems with a higher-dimensional parameter dependence, such as precessing systems, this behaviors is not anticipated in the aligned-spin case. We were able to identify the error source (inconsistent units), we were then able to produce physically reasonable covariance matrices.

The binary configuration we analyze here has the following parameters: mass ratio $q = 4$, spin magnitudes $||\vec{\chi}_1|| = 0.1$ and $||\vec{\chi}_2|| = 0.6$, inclination angle $\theta = \pi/3$, azimuthal angle $\phi = 0$, total mass $M_{total} = 12\mathrm{M}_\odot$, and initial separation $a_{init} = 40\mathrm{M}$. We find the following covariance matrix for the ($\ell = 2$)-waveforms, where in the following all (ℓ, m)-modes are computed at v^4 post-Newtonian order:

$$C = [\Gamma^{-1}] = \begin{pmatrix} 0.000102585 & -2.15201\times10^{-6} & -2.29191\times10^{-6} & 0.0000135053 \\ -2.15201\times10^{-6} & 2.20217\times10^{-6} & -4.05466\times10^{-7} & -0.0000653031 \\ -2.29191\times10^{-6} & -4.05466\times10^{-7} & 1.47451\times10^{-6} & -0.0000154815 \\ 0.0000135053 & -0.0000653031 & -0.0000154815 & 0.00401989 \end{pmatrix} \tag{22}$$

In addition, the analysis was repeated twice: 1) using all ($\ell = 2,3$)-modes as v^4 PN-order, and 2) using all ($\ell = 2,3,4$)-modes at v^4 PN-order. The resulting 2σ, or 95.4% confidence level, error ellipses for each pair of parameters are shown in Fig 1. For all the parameter planes shown in Fig. 1, the orange curve, which depicts the results when the ($\ell = 3$)-modes are included, is completely obscured by the green curve, which corresponds to the results with the inclusion of ($\ell = 4$)-modes as well. This indicates that including the ($\ell = 4$)-modes has little effect on the statistical error in this particular aligned spin case.

From the covariance matrix itself, it is clear to see that the statistical uncertainty in the inclination angle θ is much larger than the statistical uncertainty in any of the other parameters. This is clearly reflected in the $q-\theta$, $\chi_1-\theta$, and $\chi_2-\theta$ error ellipses, which show a much larger spread in θ than in the other parameters. This is especially true when higher modes are included. In each case, we see that the inclusion of the ($\ell = 3$)-modes (orange curves, hidden behind the green curves) significantly increases the statistical error in θ. Furthermore, in the $\theta-\chi_1$ error ellipse, we observe a small counter-clockwise rotation of the error ellipse with the inclusion of higher modes, which in indicates a very small correlation between the spin on the smaller black hole and the orientation of the binary. No such correlation behavior is observed for the spin on the larger black hole and θ. At this stage, we are unsure whether this is of physical origin or not and suggest that an ensemble of aligned configurations be analyzed. Further, we note that the scale of the χ_1 axis is much smaller than the scale of the θ axis, which artificially widens the ellipses along the χ_1 axis, thus somewhat exaggerating the inclination of the ellipses in that plane. However, this has no effect on the inclination of the ellipses with respect to each other, and as such does not change the fact that there exists a

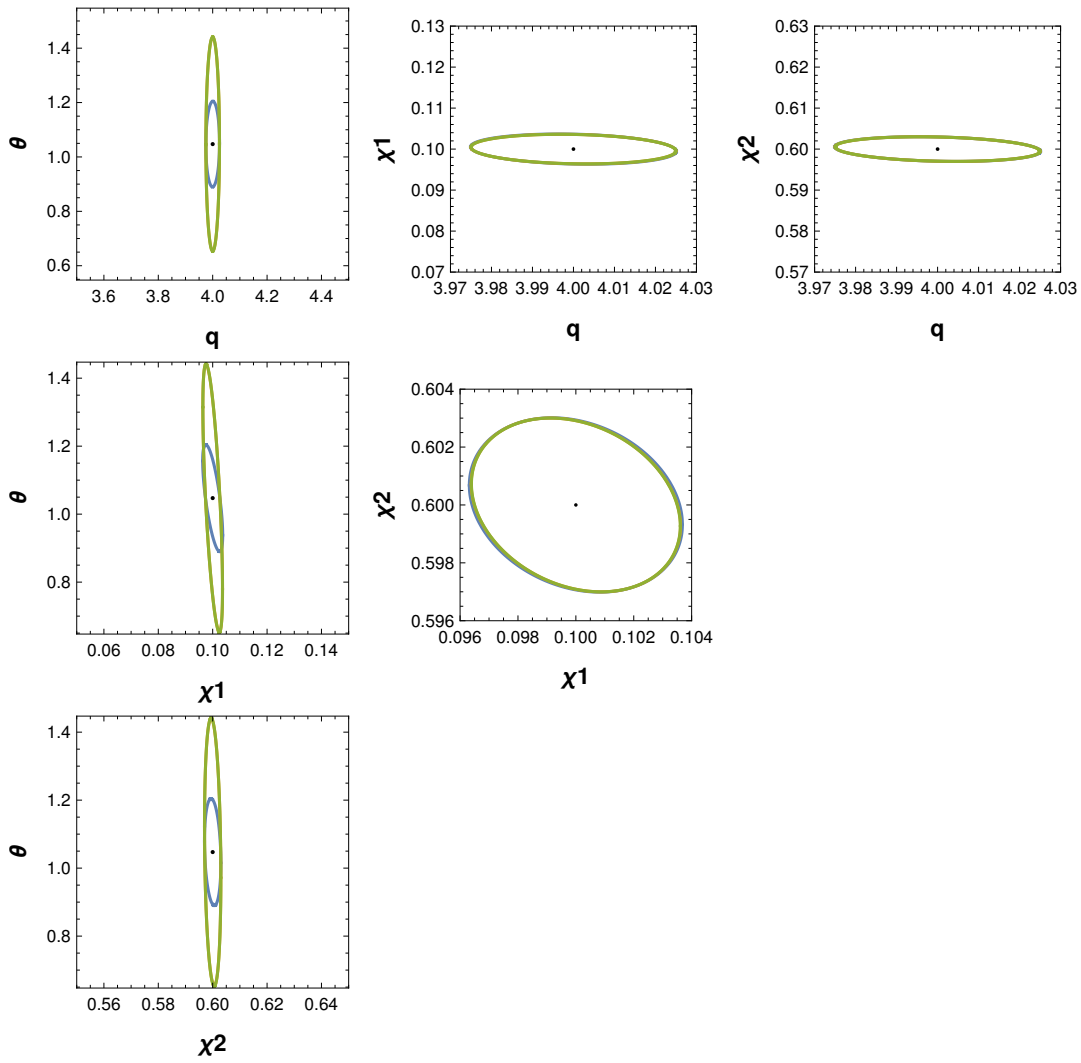

FIG. 1: 2σ confidence ellipses for each pair of parameters in the aligned spin case. The blue ellipse depict the results for the $(\ell = 2)$ waveform, the orange ellipse the $(\ell = 2,3)$ waveform, and the green ellipse the $(\ell = 2,3,4)$ waveform.

clear difference between the inclination angle of the error ellipse for the $(\ell = 2)$-waveform and inclination angle of the error ellipses for the higher-mode-inclusive waveforms.

The parameter with the second largest statistical uncertainty is the mass ratio q, while χ_1 and χ_2 have uncertainties of comparable size, as indicated both in the relatively low eccentricity of the $\chi_1 - \chi_2$ error ellipse, and in Eq. (22). Other notable features of the error ellipses in Fig. 1 include the lack of correlation, indicated by the inclination of the error ellipse, between most parameters, with the exception of $\theta - \chi_1$, as mentioned previously, and $\chi_1 - \chi_2$. The ellipses imply that the χ_1 and χ_2 parameters are most strongly correlated, while the χ_1 and θ parameters are somewhat correlated in the $(\ell = 2)$-waveform and the remaining parameters are negligibly correlated with one another, both with and without the inclusion of higher multipoles. The relatively strong correlation between χ_1 and χ_2 is rather unsurprising, as in the aligned spin case, a small, positive offset in the magnitude of χ_1 can relatively easily be compensated for with a small, negative offset in the magnitude of χ_2 to produce a similar waveform, and vice versa. This is reflected by the fact that in the aligned spin case, the two spins can be combined into one "effective" dimensionless spin parameter $\chi_{\rm eff}$ [7] given by

$$\chi_{\rm eff} = \frac{m_1\chi_1 + m_2\chi_2}{m_1 + m_2}. \tag{23}$$

The waveform of a system is unchanged if χ_1 and χ_2 change, so long as $\chi_{\rm eff}$ remains constant. There is however a very slight clockwise rotation of the error ellipse in the $\chi_1 - \chi_2$ plane with the inclusion of higher modes, which may indicate that the inclusion of higher order modes has an effect on this correlation, but the rotation is so small that we cannot as of yet make any conclusive statements about the effect of higher order modes on the $\chi_1 - \chi_2$ degeneracy in the aligned spin case.

B. Precessing case

Next, we analyzed a precessing case. At this point we decided to re-parameterize our waveforms to be a function of m_1, the mass of the smaller black hole, m_2, the mass of the larger black hole, and η, the symmetric mass ratio of the system, defined below, as opposed to just the mass ratio q.

$$\eta = \frac{m_1 m_2}{M_{total}^2}. \tag{24}$$

We again encountered problems related to ill-conditioned Fisher matrices, in particular we found negative values in the diagonal entries of the covariance matrices, which has been noted previously for precessing systems in Refs. [2, 8]. While we were able to positive definite covariance matrices for several systems, for other cases, such as cases with mass ratio $q = 6$, we found that the covariance matrix was still unphysical, which may indicate that a Fisher matrix analysis is not well-suited for some parts of the precessing binary parameter space.

Nevertheless, we successfully generated covariance matrices for a few cases, including the following system, which our analysis will be focusing on: $m_1 = 2.4$ M$_\odot$, $m_2 = 9.6$ M$_\odot$, $\eta = 0.16$, $\chi_1 = \chi_2 = (0.6,\ 0,\ 0)$, $\theta = \pi/3$, $\phi = 0$, $M_{total} = 12$ M$_\odot$ and $a_{init} = 40$ M. The parameters we varied in the Fisher analysis were the following: $\vec{\lambda} = (m_1,\ m_2,\ \eta,\ \chi_{1x},\ \chi_{1y},\ \chi_{1z},\ \chi_{2x},\ \chi_{2y},\ \chi_{2z},\ \theta)$, resulting in an 8x8 covariance matrix. We once again generated three covariance matrices for this system, one using only $(\ell = 2)$-modes to generate $h(t, \vec{\lambda})$, one using all $(\ell = 2,3)$-modes, and one using all $(\ell = 2,3,4)$-modes.

First, we consider the error ellipses in the $m_1 - m_2$ plane and in the $\chi_{1z} - \chi_{2z}$ plane, shown in Fig. 2. For these ellipses, the curve which includes the $(\ell = 2,3)$-modes is again obscured by the curve showing the results for the $(\ell = 2,3,4)$-waveform, indicating that the inclusion of $(\ell = 4)$-modes has little effect on statistical uncertainty and correlation for the parameter pairs shown in Fig. 2.

In the $m_1 - m_2$ plane, we see that the error ellipse is roughly circular, indicating that the statistical uncertainties of m_1 and m_2 are of comparable size. Also, the error ellipses for the $(\ell = 2,3)$ and $(\ell = 2,3,4)$-waveforms appear to be very slightly inside the error ellipse for the $(\ell = 2)$-waveform, potentially indicating that the inclusion of higher modes slightly improves the statistical uncertainty in m_1 and m_2.

In the $\chi_{1z} - \chi_{2z}$ plane, we see that the error ellipse is visibly inclined, indicating a strong correlation between the two parameters. This is analogous to the correlation seen between χ_1 and χ_2 in the aligned spin case, and indicates that there exists some $\chi_{\rm eff}$ value that can be used to parametrize the waveform in place of χ_{1z} and χ_{2z} in the precessing case as well. There is also a clear decrease in the statistical uncertainty in both parameters with the inclusion of higher modes, as indicated by the decreased size of the error ellipses corresponding with higher mode inclusion.

Next we consider the error ellipses between various pairs of spin components: $\chi_{1x} - \chi_{1z}$, $\chi_{1y} - \chi_{1z}$, $\chi_{2x} - \chi_{2z}$, and $\chi_{2y} - \chi_{2z}$. In each of the error ellipses shown in Fig. 3, we see that there is little to no correlation between the spin components in the plane of the orbit (i.e. the x- and y-components) and the

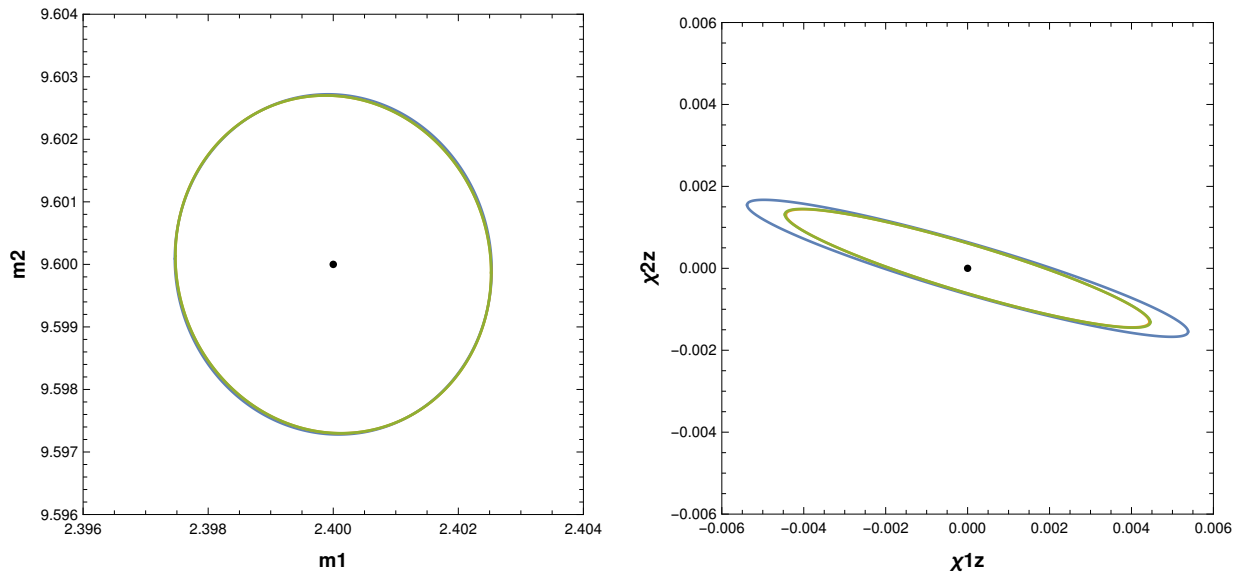

FIG. 2: The 2σ confidence ellipses in the $m_1 - m_2$ plane and the $\chi_{1z} - \chi_{2z}$ plane. Once again the blue ellipses show the results for $(\ell = 2)$ waveform, the orange ellipses for the $(\ell = 2,3)$ waveform, and the green ellipses for the $(\ell = 2,3,4)$-waveform.

spin components out of the orbital plane (i.e. the z-components) for the more massive black hole. However, there does exist a slight correlation between χ_{1x} and χ_{1z} and χ_{1y} and χ_{1z}. This correlation does however decrease with the inclusion of higher order modes, as indicated by the decreased inclination of the $(\ell = 2,3)$ and $(\ell = 2,3,4)$ error ellipses with respect to the $(\ell = 2)$ error ellipse. The observed independence between the in-plane and out-of-plane components of a single black hole's spin vector has previously been noted in Refs. [9, 10]. We also see in the $\chi_{1y} - \chi_{1z}$ plane that the inclusion of higher order modes increases the spread in χ_{1y}, but decreases the statistical uncertainty in χ_{1z}.

Next, we consider the error ellipses of the in-plane spin components (i.e. in the $\chi_{1x} - \chi_{1y}$ plane and the $\chi_{2x} - \chi_{2y}$ plane). The results are shown in Fig. 4. For the in-plane components of the less massive black hole (i.e. χ_{1x} and χ_{1y}), we see that including more higher modes results in an increased correlation between the two parameters. For the more massive black hole, however, there is little visible change in the inclination of the error ellipse with the inclusion of higher modes, but instead we see an improvement in the statistical uncertainty in both χ_{2x} and χ_{2y}.

The remaining error ellipses for this case are shown in Appendix B. In general, for the inclination angle θ we see that the inclusion of higher modes results in a slight improvement in statistical uncertainty as can be seen in the panels of Fig. 5. Furthermore, while θ is only negligibly correlated with the component masses, and not correlated with either z-components of the spins, and the y-component of the spin of the less massive black hole. However, θ is strongly correlated with all other spin component, and is slightly correlated with the symmetric mass ratio η.

We see negligible correlations between the component masses and the z-components of the spins. Furthermore, while there exists very little correlation between the component masses and the in-plane spin components, there do exist visible correlations between the symmetric mass ratio η and the spin components, particularly the x-components of both spins as can be seen in the panels in Fig. 7.

So far our analysis has only studied the effect of higher order modes on the *statistical* uncertainty of parameters for one binary case. In the upcoming weeks, we will need to both extend this analysis to a wider range of binary cases, and investigate the effect of higher order modes on *systematic* error. It is entirely possible that the uncertainties of the parameters we are studying are in fact dominated by systematic error,

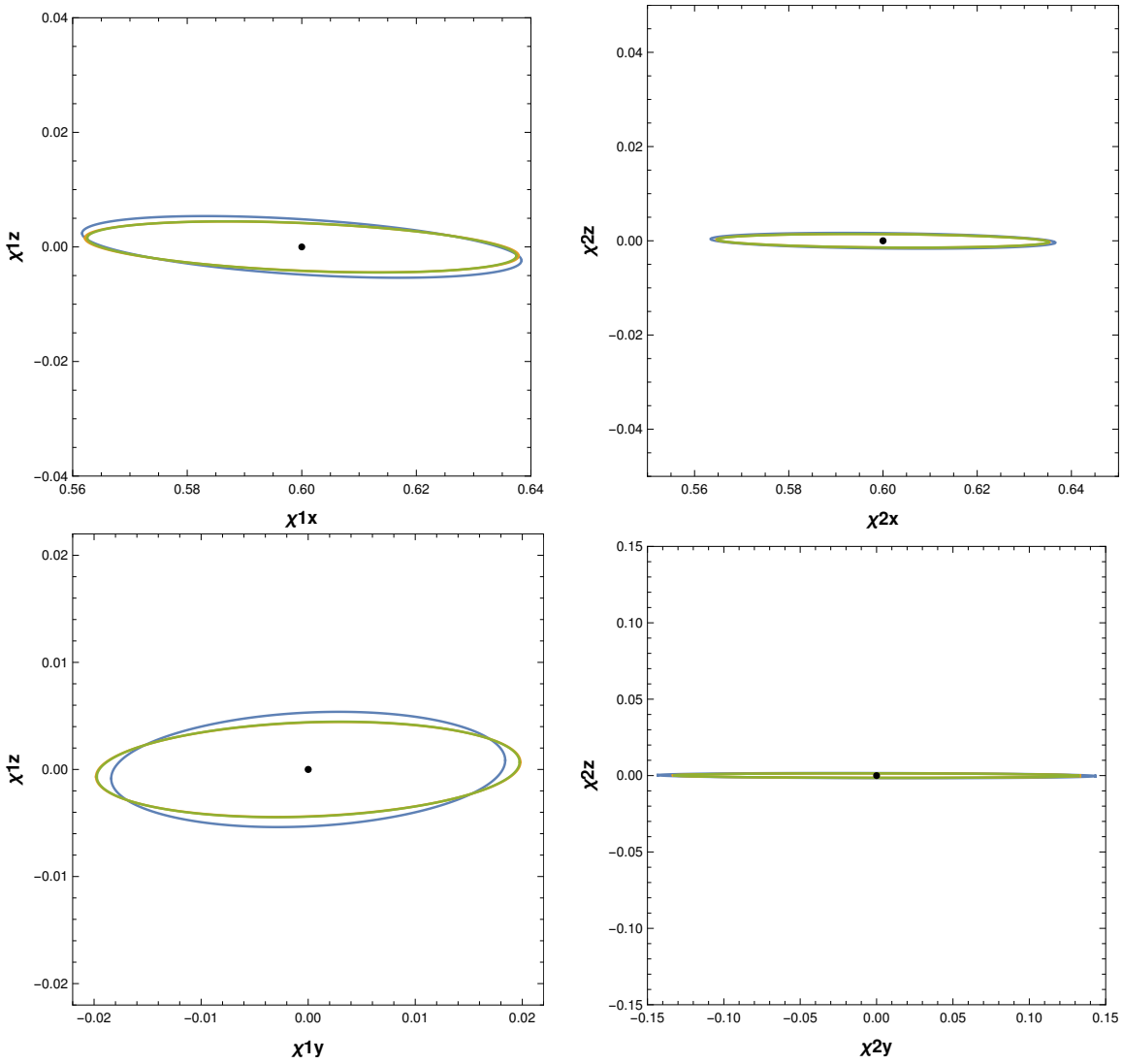

FIG. 3: The 2σ confidence ellipses in the $\chi_{1x}-\chi_{1z}$, $\chi_{1y}-\chi_{1z}$, $\chi_{2x}-\chi_{2z}$, and $\chi_{2y}-\chi_{2z}$ planes. As before, the blue ellipses shows the results for the $(\ell=2)$ waveform, the orange ellipses for the $(\ell=2,3)$ waveform, and the green ellipses for the $(\ell=2,3,4)$-waveform.

in which case the effect of higher order modes on systematic error is more relevant to parameter estimation accuracy than the effect of higher order modes on the statistical error.

C. Bayesian parameter estimation

In addition to our Fisher matrix analysis we are currently employing Bayesian parameter estimation algorithms using the LALInference software library. First, we generate a gravitational-wave signal using the post-Newtonian (PN) waveform approximation *SpinTaylorT4*. The signal is then injected into simulated, recolored Gaussian noise at a given SNR, then Bayesian statistics as described in Section II B, is used to recover the parameters of the source.

Since we are not able to directly access the $h_{\ell m}$-modes of the waveform, instead we perform a study where we truncate the post-Newtonian expansion of the waveform $h(t)$ at different PN orders v^n, where v is

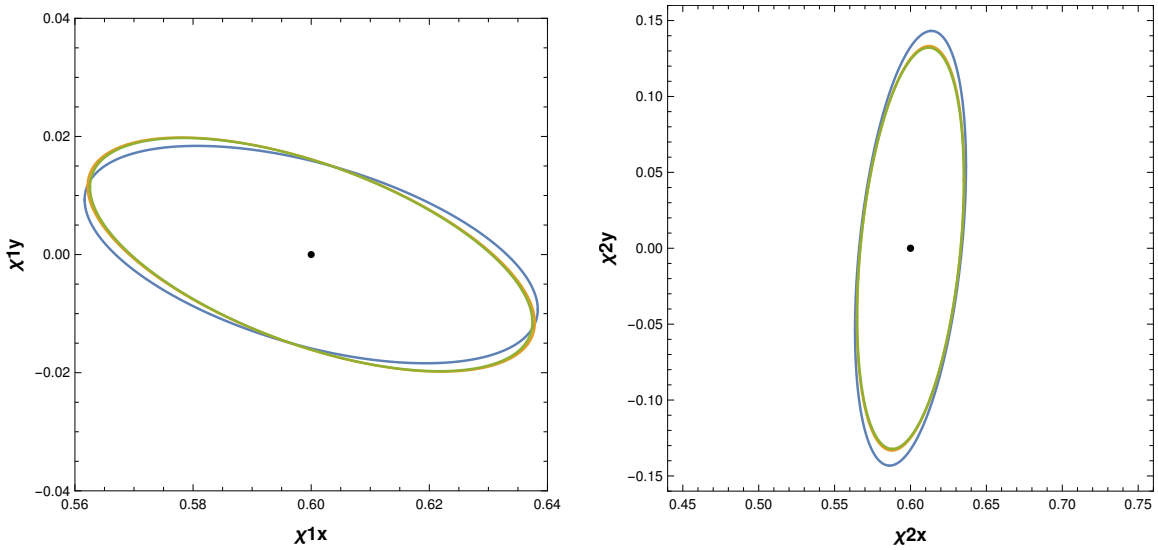

FIG. 4: The 2σ confidence ellipses in the $\chi_{1x}-\chi_{1y}$ and $\chi_{2x}-\chi_{2y}$ planes. The blue ellipses corresponds with the $(\ell=2)$ waveform, the orange ellipses correspond with the $(\ell=2,3)$ waveform, and the green ellipses correspond with the $(\ell=2,3,4)$-waveform.

the PN expansion parameter:

$$h(t)=A(t,v^m)e^{i\phi(t,v^n)}, \tag{25}$$

where $A(t,v^m)$ is the GW amplitude at a specific PN order m and $\phi(t,v^n)$ denotes the GW phase at the PN order n.

The binary configuration is the same low-mass, precessing black hole system as before: mass ratio $q=4$, spins $\chi_1=\chi_2=(0.6,\ 0,\ 0)$, total mass $M_{total}=12\ \mathrm{M}_\odot$, initial separation $a_{init}=40\,M$, inclination angle $\theta=\pi/3$, and azimuthal angle $\phi=0$. The injected waveform has an SNR of $\rho=8$, and PN order of 3.5, i.e. $O(v^7)$, in both amplitude and phase. The template waveforms used for parameter recovery, on the other hand, have PN order of 0 in amplitude, and PN order of 3.5 in the phase.

While it is not possible for us to directly map the PN order of the waveform's amplitude and phase to a spherical harmonic mode distribution, through these runs we can do an additional study on whether using a lower PN order in amplitude results in parameter biases. Since this is how parameter recovery is typically done for low-mass systems with LIGO, this will give us useful information about how well lower order PN approximations constrain parameters for precessing systems, and whether or not the parameter accuracy can be improved when higher order PN amplitudes are used.

IV. NEXT STEPS

We will now move on to investigating the systematic error that arises from using a quadrupole $(\ell=2,\ \mathrm{m}=\pm2)$ waveform or an $(\ell=2)$ waveform as opposed to a higher-mode inclusive waveform during parameter estimation. We do so using Eq. (19), for which we will need the Fisher matrix and overlap code we have already implemented, in addition to a likelihood-optimization code, which we will need to find the maximum likelihood estimate $\vec{\lambda}'$. For this we will most likely use the `NMaximize` function in `Mathematica` to numerically optimize the likelihood function over the parameter space. Because our parameter space is ten dimensional, it is possible for the likelihood function over the parameter space to be muli-modal, so we will have to ensure that whatever numerical maximization algorithm we use does not return a local maximum as opposed to a global maximum. We will most likely use the

`DifferentialEvolution` method option in `Mathematica`'s `NMaximize` function to this end. We will also continue to investigate ways to improve our Fisher matrix analysis to prevent ill-conditioned covariance matrices, as our current implementation produces unphysical covariance matrices for, among others, the $q = 6$ case. The $q = 6$ case is of particular interest to us, as our match calculations for this case indicated potential improvements in parameter estimation through the inclusion of higher modes. We have also set up a few parameter estimations runs in the LALInference software library, and once those runs are complete we can begin to analyze the resulting data.

Appendix A: Mathematica Implementation of Overlap

The code to calculate the overlap between two waveforms h_1 and h_2 has been written in `Mathematica`. The overlap is calculated by fixing the polarization angles $\psi \equiv \sigma$ and providing time series data $h_1(t)$ and $h_2(t)$. The noise curve is provided as a frequency series for $S_n(f)$ in units of $\left[\mathrm{Hz}^{-1}\right]$. Algorithmically, the overlap is calculated in the following steps:

1. Compute the complex GW strains for a given orientation (θ, ϕ):

$$h_{i,\,\mathrm{strain}}(t;\theta,\phi) = \sum_{\ell=2}^{\infty} \sum_{m=-\ell}^{\ell} h_{i,\ell m}(t)\, {}_{-2}Y_{\ell m},(\theta,\phi) \tag{A1}$$

   with $i = 1, 2$.

2. Convert the time values in each time series from units of M to units of seconds.

3. Calculate the dimensionful Fourier transforms, $\tilde{h}_1$ and $\tilde{h}_2$ using the `Fourier` function in Mathematica and multiplying the output by Δt, where Δt is the time interval in seconds. Note that we must set the `FourierParameters` flag equal to $(1, 1)$ as we use non-unitary Fourier conventions in our analysis.

4. Set $f_{\mathrm{min}} = 10\,\mathrm{Hz}$ and $f_{\mathrm{max}} = M f_{\mathrm{ISCO}} * \texttt{scale}$, where $M f_{\mathrm{ISCO}}$ is the frequency in units of M of the innermost stable circular orbit (ISCO) and `scale` converts the frequency from units of M (the total mass of the system in solar masses) to units of Hz. We then take all values in $\tilde{h}_1$ and $\tilde{h}_2$ that correspond with frequencies $f_{\mathrm{min}} < f < f_{\mathrm{max}}$. $M f_{\mathrm{ISCO}}$ is given by:

$$M f_{\mathrm{ISCO}} = \frac{1}{\pi \sqrt{6}^3}, \tag{A2}$$

   which for the considered configurations corresponds to $\sim 368\mathrm{Hz}$.

5. Evaluate $S_n(f)$ at each frequency in the list.

6. Generate two lists of values:

$$L1 = \frac{\tilde{h}_1(f)\,\tilde{h}_2^*(f)}{S_n(f)} \qquad \text{and} \qquad L2 = \frac{\tilde{h}_1^*(-f)\,\tilde{h}_2^*(f)}{S_n(f)}. \tag{A3}$$

7. We can efficiently calculate the two integrals in Eq. (5) at various time shifts by taking the IFFT, given by the `InverseFourier` function in Mathematica, of $L1$ and $L2$, remember to set `FourierParameters` equal to $(-1, 1)$.

8. As both waveforms have the same polarization angle ψ, we can now calculate the final overlap maximized over the time shifts by evaluating

$$Max@Re[\,\mathrm{InverseFourier[L1]} + \mathrm{InverseFourier[L2]}\, e^{4i\psi}\,]. \tag{A4}$$

Appendix B: Additional Error Ellipses

1. Error Ellipses for Inclination Angle θ

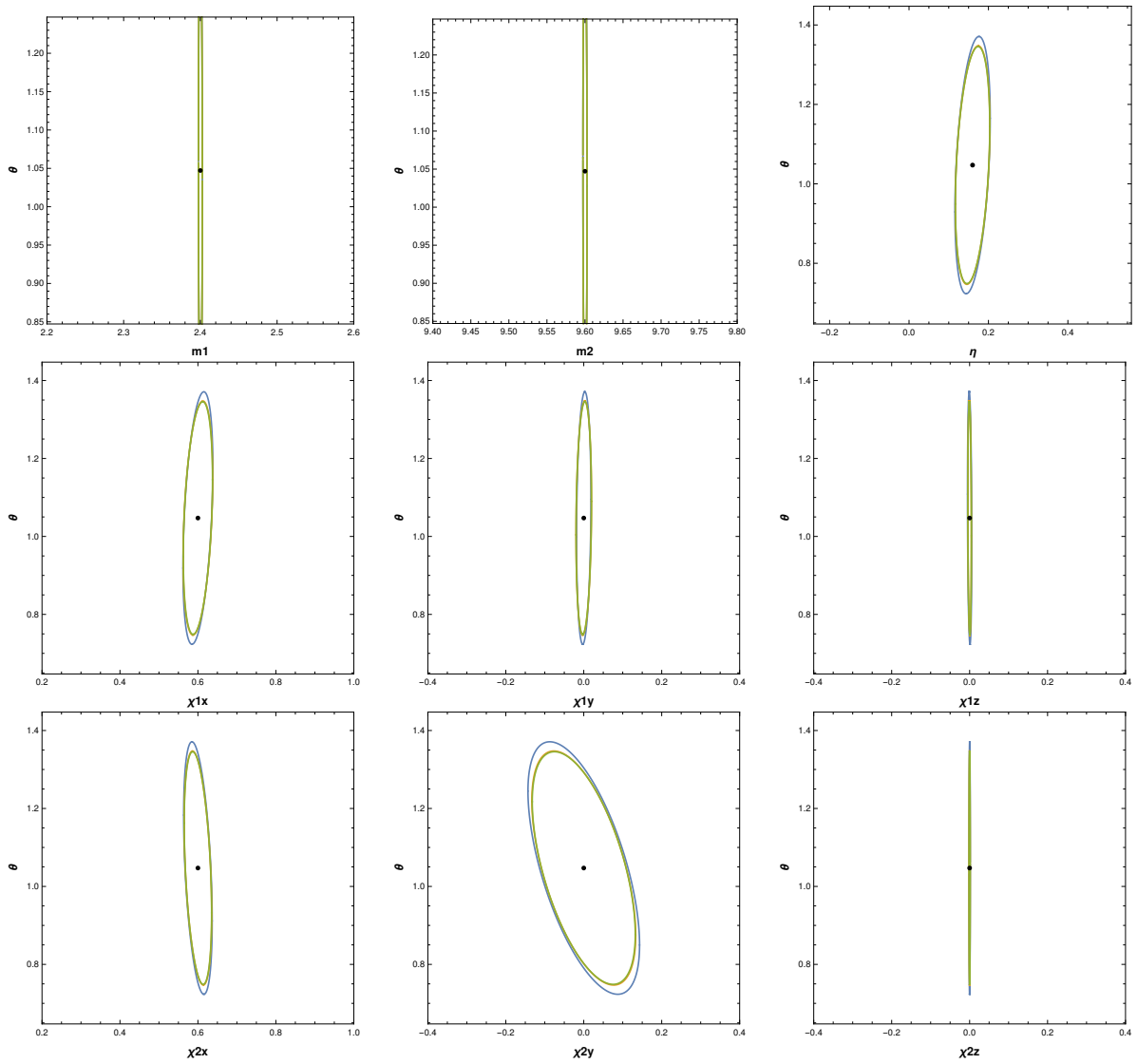

FIG. 5: All 2σ confidence ellipses corresponding with the inclination angle of the binary θ for the precessing system used in Sec. III. The blue ellipses show the results for the $(\ell = 2)$ waveform, the orange ellipses for the $(\ell = 2, 3)$ waveform, and the green ellipses for the $(\ell = 2, 3, 4)$-waveform.

2. Error Ellipses for Spin Components and Mass Parameters

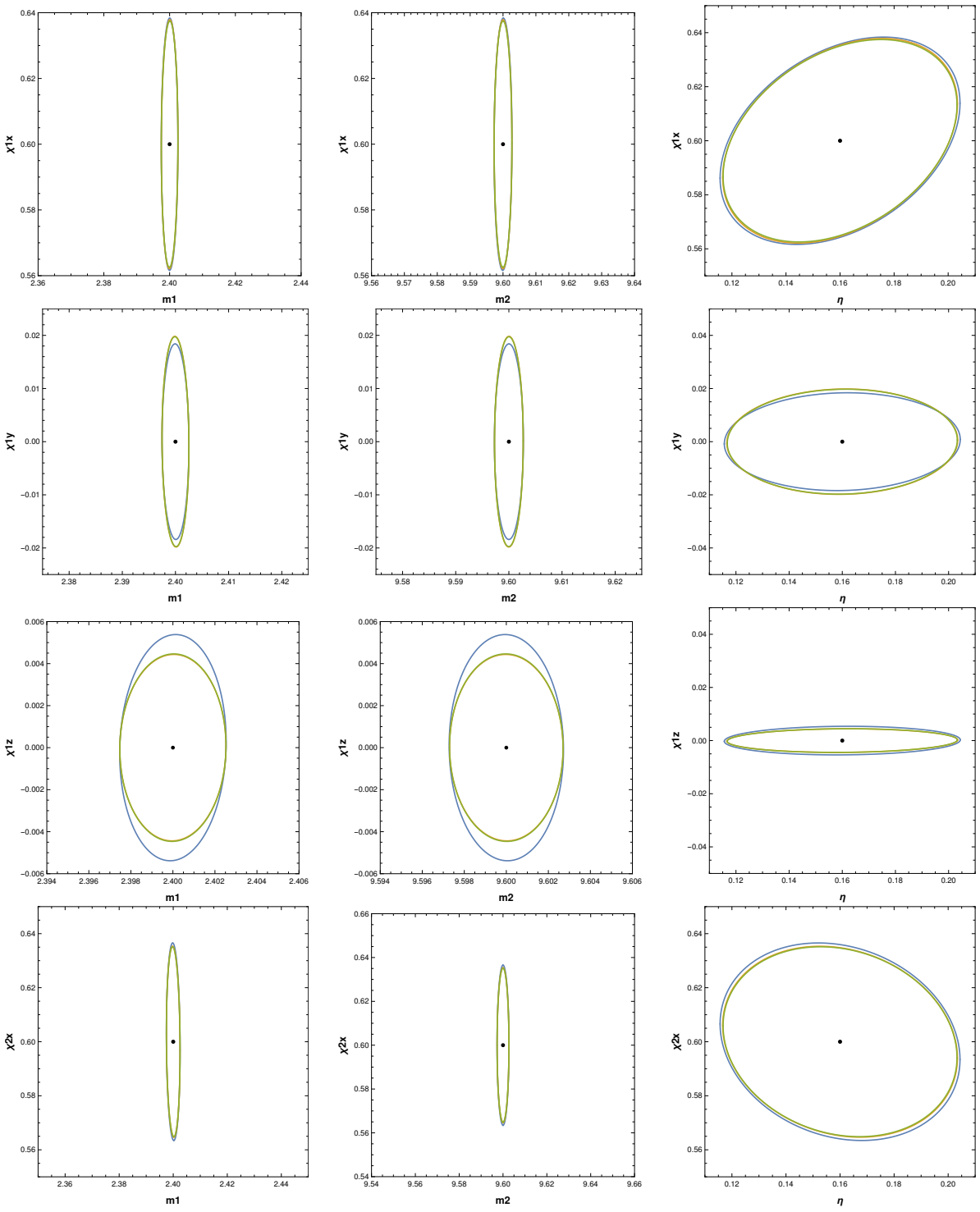

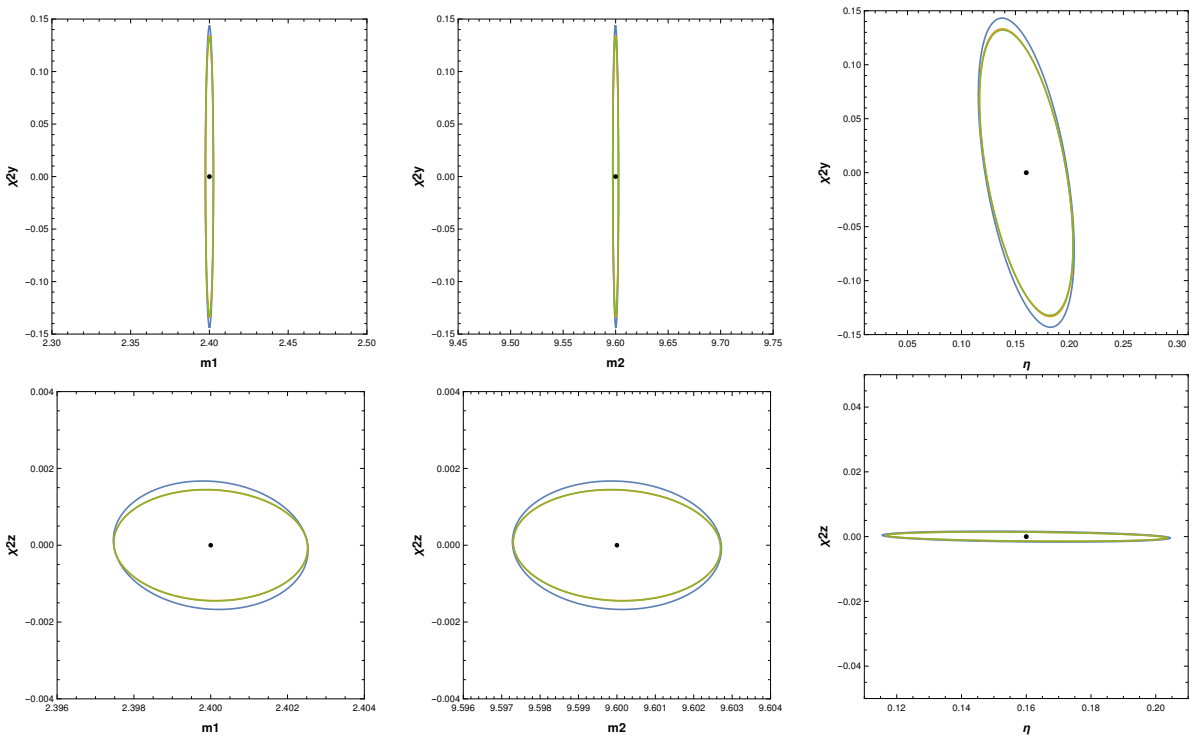

FIG. 7: All 2-σ confidence ellipses in the plane of a spin component and a mass parameter for the precessing system as discussed in Sec. III. The blue ellipses show the results for the $(\ell = 2)$ waveform, the orange ellipses for the $(\ell = 2,3)$ waveform, and the green ellipses for the $(\ell = 2,3,4)$-waveform.

[1] Patricia Schmidt, Frank Ohme, and Mark Hannam. Towards models of gravitational waveforms from generic binaries: Ii. modelling precession effects with a single effective precession parameter. *Phys. Rev. D*, 91:024043, Jan 2015.

[2] Hee-Suk Cho, Evan Ochsner, Richard O'Shaughnessy, Chunglee Kim, and Chang-Hwan Lee. Gravitational waves from black hole-neutron star binaries: Effective Fisher matrices and parameter estimation using higher harmonics. *Phys. Rev.*, D87(2):024004, 2013.

[3] D. Coe. Fisher Matrices and Confidence Ellipses: A Quick-Start Guide and Software. *ArXiv e-prints*, June 2009.

[4] Frank Ohme. *Bridging the Gap between Post-Newtonian Theory and Numerical Relativity in Gravitational-Wave Data Analysis*. PhD thesis, Potsdam, Max Planck Inst., 2012.

[5] Vijay Varma, Parameswaran Ajith, Sascha Husa, Juan Calderon Bustillo, Mark Hannam, and Michael Pürrer. Gravitational-wave observations of binary black holes: Effect of nonquadrupole modes. *Phys. Rev. D*, 90:124004, Dec 2014.

[6] J. Veitch et al. Parameter estimation for compact binaries with ground-based gravitational-wave observations using the LALInference software library. *Phys. Rev.*, D91(4):042003, 2015.

[7] P. Ajith et al. Inspiral-merger-ringdown waveforms for black-hole binaries with non-precessing spins. *Phys. Rev. Lett.*, 106:241101, 2011.

[8] Frank Ohme, Alex B. Nielsen, Drew Keppel, and Andrew Lundgren. Statistical and systematic errors for gravitational-wave inspiral signals: A principal component analysis. *Phys. Rev.*, D88(4):042002, 2013.

[9] Mark Hannam, Patricia Schmidt, Alejandro Bohé, Leïla Haegel, Sascha Husa, Frank Ohme, Geraint Pratten, and Michael Pürrer. Simple Model of Complete Precessing Black-Hole-Binary Gravitational Waveforms. *Phys. Rev. Lett.*, 113(15):151101, 2014.

[10] Patricia Schmidt, Mark Hannam, and Sascha Husa. Towards models of gravitational waveforms from generic

binaries: A simple approximate mapping between precessing and non-precessing inspiral signals. *Phys. Rev.*, D86:104063, 2012.

[11] We refer to the angle between total angular momentum and the line-of-sight as the inclination angle θ.